Effects of poloidal sheared flow and active feedback on tokamak edge fluctuations

1993 Nucl. Fusion 33 1009

(http://iopscience.iop.org/0029-5515/33/7/I04)

EFFECTS OF POLOIDAL SHEARED FLOW AND ACTIVE FEEDBACK ON TOKAMAK EDGE FLUCTUATIONS

R. SINGH, P.K. KAW, A. SEN, G.C. SETHIA
Institute for Plasma Research,
Bhat, Gandhinagar, India

ABSTRACT. The influence of sheared poloidal flow and of a phase sensitive feedback source on the various edge instabilities of tokamaks are investigated. The conditions for stabilization of the rippling mode, for the drift dissipative mode and for the radiative condensation instability are obtained from detailed numerical solutions and from approximate analytic solutions of the relevant eigenmode equations.

1. INTRODUCTION

It is widely believed now that the overall energy and particle confinement in a tokamak discharge are strongly influenced by fluctuations in the tokamak edge [1–3]. Methods to control the level of these fluctuations are therefore of great interest in tokamak physics. Recent experiments [4–6] have demonstrated that the introduction of a sheared poloidal flow, either by external biased probes or by natural processes driving the H mode [7], can have a significant stabilizing influence on fluctuations in the tokamak edge. Similarly, the use of phase sensitive feedback methods to stabilize low frequency fluctuations in a laboratory plasma, has received wide experimental verification [8]. However, such methods have not yet been attempted in tokamaks, perhaps because the tokamak edge turbulence is typically broadband. Although the most appropriate method of stabilizing such fluctuations using feedback would be one of the recently developed chaos control techniques [9], there are two reasons why the simpler feedback techniques should be attempted and may lead to interesting results. Firstly, it appears that the particle confinement time is largely governed by a relatively small band of low frequency long wavelength fluctuations and this small band may be amenable to feedback stabilization. Secondly, the edge region is readily accessible to, for example, probes and limiter bias potentials, and so feedback methods could be readily implemented. Proposals to carry out such experiments, therefore, already exist [10].

The important mechanisms that may be responsible for the observed edge fluctuations in a tokamak are:

(i) Rippling instabilities that are driven by resistivity gradients associated with temperature and/or impurity density gradients in the plasma;

(ii) Radiative condensation instabilities that arise owing to the dependence of the radiative capacity L on the density and temperature ($L \propto n^2$ and $\partial L/\partial T < 0$);

(iii) The drift dissipative instability driven by pressure gradients and depending on the parallel resistivity to give a phase difference between $\tilde{n}$ and $\tilde{\phi}$ (which is necessary for wave growth).

In this paper we have examined the influence of poloidal velocity shear and a phase sensitive feedback source in the electron continuity equation (and hence in the charge neutrality condition) on the linear growth of the above mentioned three instabilities. Taking account of magnetic shear, a simple model of velocity shear and the dependence of ω_* on x (the radial distance $r - r_s$ from a mode rational surface), the slab model eigenmode equations have been set up in each case. These equations are solved numerically, employing a shooting technique. A detailed analysis of the mode stability is presented. The numerical results are further supported by analytical solutions obtained in limiting cases using, for example, perturbation theory, the WKB approach, matched asymptotic schemes. A preliminary account of this work was presented in Ref. [11], where the basic equations were derived and some analytic approximations worked out. Other related work, which has recently appeared in the literature, is that of Sugama et al. [12], where the authors have looked at the effect of poloidal velocity shear on resistive interchange modes that may be unstable in stellarators and heliotrons.

The paper is organized as follows: in Section 2, we discuss the basic physical model and derive a generalized set of equations governing the evolution of the rippling, drift dissipative, and radiative condensation instabilities. These modes are then individually analysed in Sections 3.1, 3.2 and 3.3, respectively. In each case the generalized equations of Section 2 are used to obtain an eigenmode equation for the modes concerned which is then solved both numerically and analytically in certain limits. Detailed stability results including analytic expressions for modified growth rates are presented and conditions for stabilization discussed. Section 4 summarizes the main conclusions of our work.

2. BASIC EQUATIONS

We first give a general treatment for rippling, radiative condensation and drift dissipative instabilities, using the Braginksii two fluid equations [13]. For simplicity, we model the tokamak plasma in the straight cylindrical approximation with a periodicity in the z direction. The equilibrium density, temperature, magnetic shear, resistivity and $Z_{\rm eff}$ profiles are taken to have a radial variation. The equilibrium electric field is also assumed to be in the radial direction, that is $\boldsymbol{E} = -\hat{e}_r\nabla\phi_0$. For the low frequency modes we are considering and in the region of the tokamak edge plasma it is also appropriate to choose the ordering $\omega \ll \Omega_{\rm i}$, $a_{\rm i} \ll L$, $\nu_{\rm ei} \ll \Omega_{\rm i}$, where $\Omega_{\rm i}$ is the ion gyrofrequency, $a_{\rm i}$ $(= c_{\rm i}/\Omega_{\rm i})$ is the ion Larmor radius, $c_{\rm i}$ is the ion thermal velocity, $\nu_{\rm ei}$ is the electron–ion collision frequency and L is a typical equilibrium scale length. We assume the equilibrium ion and electron perpendicular flow velocities to be of the order of the speed of sound. Then, from the momentum equations we obtain,

$$\boldsymbol{v}_{\perp j} = \frac{c}{B}\left(\hat{\boldsymbol{b}} \times \nabla\phi_0 + \frac{\hat{\boldsymbol{n}} \times \nabla P_j}{e_j N}\right) \tag{1}$$

where $\hat{\boldsymbol{b}} = \boldsymbol{B}/B$, ϕ_0 is the equilibrium electrostatic potential, N is the equilibrium plasma density and j = e(electrons), i(ions). The equilibrium parallel flow velocities may be approximated as

$$\frac{\hat{\boldsymbol{n}}\cdot(\boldsymbol{v}_{\rm e} - \boldsymbol{v}_{\rm i})}{C_{\rm s}} = \left(\frac{e\hat{\boldsymbol{n}}\cdot\boldsymbol{E}L}{T_{\rm e}}\right)\left(\frac{m_{\rm i}}{m_{\rm e}}\right)\left(\frac{\Omega_{\rm i}a_{\rm s}}{\nu_{\rm ei}L}\right) \tag{2}$$

where $\hat{\boldsymbol{n}}\cdot\boldsymbol{E}$ is the applied toroidal electric field, $a_{\rm s} = C_{\rm s}/\Omega_{\rm i}$ and $C_{\rm s}$ is the sound speed. We take linear perturbations to vary as

$$\tilde{\phi} \sim \phi(x)\exp(-{\rm i}\omega t + {\rm i}m\theta + {\rm i}l\phi)$$

where $x = r - r_{\rm s}$ is the distance away from the mode rational surface $m - lq(r_{\rm s}) = 0$ around which the modes are assumed to be localized. The parallel wave vector in a sheared magnetic field can be written as

$$\hat{\boldsymbol{n}}\cdot\nabla = {\rm i}k_\parallel' x;\ k_\parallel' = k_\theta/L_{\rm s},\ L_{\rm s} \simeq q(r_{\rm s})R \text{ and } k_\theta = m/r_{\rm s}$$

We also neglect the effects of ion gyroviscosity and parallel ion viscosity on the grounds that

$$(\nu_{\rm ii}/\omega)(a_{\rm s}/x)^4 \ll 1$$

$$\left(\frac{\omega m_{\rm i}}{\nu_{\rm ei}m_{\rm e}}\right)\left(\frac{L_N}{L_{\rm s}}\right)^2\left(\frac{\omega_*}{\omega}\right)^2\sqrt{\frac{m_{\rm e}}{m_{\rm i}}}\left(\frac{x}{a_{\rm s}}\right)^2 \ll 1$$

where $L_N^{-1} = -{\rm d}\ln N/{\rm d}r$. This is based on the assumption that the mode widths of the rippling, drift dissipative and radiation condensation modes are such that $x/a_{\rm s} > 1$. We shall justify this fact a posteriori. For the low β edge plasma, it is also appropriate to neglect the magnetic field fluctuations. Taking the curl of the momentum equations and dotting with $\hat{n}$ gives

$$\begin{aligned} a_{\rm s}^2\left(\frac{\partial}{\partial t} + \boldsymbol{v}_{\rm i}\cdot\nabla\right)\nabla_\perp^2\left(\tilde{\phi} + \frac{\tilde{p}_{\rm i}}{\tau}\right) &= a_{\rm s}^2\left(-\frac{v_0'}{L_N} + v_0''\right)\frac{1}{r}\frac{\partial}{\partial\theta}\left(\tilde{\phi} + \frac{\tilde{p}_{\rm i}}{\tau}\right) \\ &+ \left(\frac{\partial}{\partial t} + \boldsymbol{v}_0\cdot\nabla\right)\tilde{n}_{\rm i} + \frac{a_{\rm s}C_{\rm s}}{L_N}\frac{1}{r}\frac{\partial}{\partial\theta}\tilde{\phi} \\ &+ \frac{1}{N}\hat{n}\cdot\nabla(Nv_{\parallel{\rm i}}) \end{aligned} \tag{3}$$

$$\begin{aligned} 0 = &-\left(\frac{\partial}{\partial t} + \boldsymbol{v}_0\cdot\nabla\right)\tilde{n}_{\rm e} + S_{\rm e}(\omega)\tilde{n}_{\rm e} \\ &- \frac{a_{\rm s}C_{\rm s}}{L_N}\frac{1}{r}\frac{\partial}{\partial\theta}\tilde{\phi} - \frac{1}{N}\hat{n}\cdot\nabla(Nv_{\parallel{\rm e}}) \end{aligned} \tag{4}$$

where $\tilde{\phi} = e\phi/T_{\rm e}$, $\tilde{n} = n/N$, $\boldsymbol{v}_{\rm j} \simeq -c(E_r/B)\hat{e}_\theta = \boldsymbol{v}_0$, $v_0' = {\rm d}v_0/{\rm d}r$, $\tau = T_{\rm e}/T_{\rm i}$ and we have assumed the $\boldsymbol{E} \times \boldsymbol{B}$ and diamagnetic drifts to be the dominant perturbed velocities. In deriving the above equations we have used the ion continuity equation and the electron continuity equation in the presence of a phase sensitive feedback source term $S_{\rm e}(\omega)$. In Eq. (4) the electron inertia term has been neglected.

The sum of the parallel electron and ion momentum equations yields

$$m_{\rm i}N\left(\frac{\partial}{\partial t} + \boldsymbol{v}_0\cdot\nabla\right)v_{\parallel{\rm i}} = -P_{\rm e}\nabla_\parallel\left(\tilde{p}_{\rm e} + \frac{\tilde{p}_{\rm i}}{\tau}\right) \tag{5}$$

and the parallel component of the electron momentum equation is

$$\begin{aligned} \frac{\nabla_\parallel\tilde{j}_\parallel}{eN} = &-\frac{T_{\rm e}}{e^2N\eta}\nabla_\parallel^2(\tilde{\phi} - \tilde{p}_{\rm e} - 0.71\tilde{t}_{\rm e}) \\ &- \frac{J_\parallel}{eN}\nabla_\parallel(\tilde{\eta}_{\rm sp} + \tilde{Z}_{\rm eff}) \end{aligned} \tag{6}$$

where $\tilde{\eta} = \tilde{\eta}_{\rm sp} + \tilde{Z}_{\rm eff}$, $\tilde{\eta}_{\rm sp} = \eta_{\rm sp}/\eta_{\rm sp0} = -3\tilde{t}_{\rm e}/2$ (subscript sp stands for Spitzer resistivity), $\tilde{t}_{\rm e} = t_{\rm e}/T_{\rm e}$, $\tilde{Z}_{\rm eff} = z_{\rm eff}/Z_{\rm eff0}$, $\eta_{\rm sp0} = 0.51m_{\rm e}\nu_{\rm ei}/Ne^2$, $\tilde{p}_j = p_j/P_j$, $\tau = T_{\rm e}/T_{\rm i}$ and $J_\parallel = -eNv_{\parallel{\rm e}}$. The $Z_{\rm eff}$ dynamics can be described by

$$\left(\frac{\partial}{\partial t} + v_0\cdot\nabla - \chi_z\nabla_\parallel^2\right)\tilde{Z}_{\rm eff} = -\frac{a_s C_s}{L_z}\frac{1}{r}\frac{\partial}{\partial\theta}\tilde{\phi} \tag{7}$$

where the χ_z is the impurity diffusivity [14] along the field lines. Finally, the electron and ion energy equations are

$$\frac{3}{2}NT_e\left(\frac{\partial}{\partial t} + v_0\cdot\nabla\right)\tilde{t}_e = -\frac{3}{2}NT_e\frac{a_s C_s}{|L_T|}\frac{1}{r}\frac{\partial}{\partial\theta}\tilde{\phi}$$
$$+ P_e\frac{\nabla_\parallel\tilde{j}_\parallel}{eN} - P_e\nabla_\parallel v_{\parallel i}$$
$$+ 0.71P_e\frac{\nabla_\parallel\tilde{j}_\parallel}{eN} + T_e\chi_{\parallel e}\nabla_\parallel^2\tilde{t}_e$$
$$+ T_e\chi_{\perp e}\nabla_\perp^2\tilde{t}_e - 3\frac{m_e}{m_i}\nu_{ei}P_e\left(\tilde{t}_e - \frac{\tilde{t}_i}{\tau}\right)$$
$$- P_e\left(\frac{2L}{NT_e}\tilde{n} + \frac{1}{N}\frac{\partial L}{\partial T_e}\tilde{t}_e\right) \tag{8}$$

and

$$\frac{3}{2}NT_i\left(\frac{\partial}{\partial t} + v_0\cdot\nabla\right)\tilde{t}_i$$
$$= -\frac{3}{2}NT_i\frac{a_s C_s}{|L_{T_i}|}\frac{1}{r}\frac{\partial}{\partial\theta}\tilde{\phi} + P_i\nabla_\parallel v_{\parallel i} - T_i\chi_{\parallel i}\nabla_\parallel^2\tilde{t}_i$$
$$+ T_i\chi_{\perp i}\nabla_\perp^2\tilde{t}_i + 3\frac{m_e}{m_i}\nu_{ei}P_i(\tau\tilde{t}_e - \tilde{t}_i) \tag{9}$$

where the χ_j are the electron and ion thermal conductivities [13]. The above equations complete the model equations for the descriptions of the low frequency edge plasma modes. They can be combined and expressed in a non-dimensional form by the following set of equations:

$$\nabla_\perp^2\tilde{\phi} = -\frac{k_\theta}{\bar{\omega}}\left(-\frac{a_s}{L_N}v_0'(\xi) + v_0''(\xi)\right)\tilde{\phi}$$
$$+ i\frac{S_e}{\bar{\omega}}\tilde{n} + i\frac{\xi^2}{\xi_R^2}(\tilde{\phi} - \tilde{n} - 1.71\tilde{t}_e)$$
$$- a_1\xi\tilde{t}_e + g_1(\xi)a_2\xi\tilde{\phi} \tag{10}$$

$$\tilde{n} = \nabla_\perp^2\tilde{\phi} + \frac{k_\theta}{\bar{\omega}}\left(-\frac{a_s}{L_N}v_0'(\xi) + v_0''(\xi)\right)\tilde{\phi} + \frac{\omega_*}{\bar{\omega}}\tilde{\phi}$$
$$+ \frac{\xi^2}{\xi_s^2}\left[\tilde{n}\left(1 + \frac{1}{\tau}\right) + \frac{\tilde{t}_i}{\tau} + \tilde{t}_e\right] \tag{11}$$

$$\tilde{t}_e = \eta_e\frac{\omega_*}{\bar{\omega}}\tilde{\phi} + \frac{2}{3}\frac{\xi^2}{\xi_s^2}\left[\tilde{n}\left(1 + \frac{1}{\tau}\right) + \frac{\tilde{t}_i}{\tau} + \tilde{t}_e\right]$$
$$- i\frac{\xi^2}{\xi_{k\parallel e}^2}\tilde{t}_e + \frac{i}{\xi_{k\perp e}^2}\nabla_\perp^2\tilde{t}_e - i\hat{\gamma}_n\tilde{n} + i\hat{\gamma}_T\tilde{t}_e$$
$$- i\hat{\gamma}_{ei}\left(\tilde{t}_e - \frac{\tilde{t}_i}{\tau}\right) - 1.14\left[-i\frac{\xi^2}{\xi_R^2}(\tilde{\phi} - \tilde{n} - 1.71\tilde{t}_e)\right.$$
$$\left.+ a_1\xi\tilde{t}_e - g_1(\xi)a_2\xi\tilde{\phi}\right] \tag{12}$$

$$\tilde{t}_i = \eta_i\frac{\omega_*}{\bar{\omega}}\tilde{\phi} + \frac{2}{3}\frac{\xi^2}{\xi_s^2}\left[\tilde{n}\left(1 + \frac{1}{\tau}\right) + \frac{\tilde{t}_i}{\tau} + \tilde{t}_e\right]$$
$$- i\frac{\xi^2}{\xi_{k\parallel i}^2}\tilde{t}_i + \frac{i}{\xi_{k\perp i}^2}\nabla_\perp^2\tilde{t}_i + i\tau\hat{\gamma}_{ei}\left(\tilde{t}_e - \frac{\tilde{t}_i}{\tau}\right) \tag{13}$$

where the prime means differentiation with respect to ξ, $S_e = |S_e(\omega)|\exp(i\phi)$ is a phase sensitive feedback source in the continuity equation, $\xi = x/a_s$, $\nabla_\perp^2 = \partial^2/\partial\xi^2 - k_\theta^2 a_s^2$, $\xi_R^2 = 0.51\bar{\omega}\nu_{ei}/k_\parallel'^2 C_e^2 a_s^2$, $C_j^2 = T_j/m_j$, $g_1 = -i\xi_z^2(\xi^2 - i\xi_z^2)^{-1}$ takes account of impurity diffusion along the field lines, $\xi_z^2 = Z^2\bar{\omega}\nu_{ii}/k_\parallel'^2 C_i^2 a_s^2$, $\bar{\omega} = \omega - k_\theta v_0(\xi)$, $a_1 = 3J_\parallel k_\parallel' a_s/2eN\bar{\omega}$, $a_2 = (J_\parallel k_\parallel' a_s/2eN\bar{\omega})(\omega_* L_N/\bar{\omega}L_z)$ (takes account of the impurity gradient) $L_z^{-1} = -\mathrm{d}\ln Z_{\rm eff}/\mathrm{d}r$, $\omega_* = k_\theta a_s C_s/L_N$, $\xi_s^2 = \bar{\omega}^2/k_\parallel'^2 C_s^2 a_s^2$, $\xi_{k\parallel e}^2 = 0.95\bar{\omega}\nu_{ei}/k_\parallel'^2 C_e^2 a_s^2$, $\xi_{k\perp j}^2 = (3/2)N\bar{\omega}a_s^2/\chi_{\perp j}$, $\hat{\gamma}_n = (4/3)(L/NT_e\bar{\omega})$, $\hat{\gamma}_T = -(2/3)(1/\bar{\omega}N)(\partial L/\partial T_e)$, $\hat{\gamma}_{ei} = 2(m_e/m_i)(\nu_{ei}/\bar{\omega})$, $\xi_{k\parallel i}^2 = (3/2)(N\bar{\omega}/\chi_{\parallel i}k_\parallel'^2 a_s^2)$ and the definitions of the heat diffusion coefficients $\chi_{\parallel j}$ and $\chi_{\perp j}$ follow from Braginskii [13]. Equations (10)–(13) may now be utilized to derive the eigenmode equations for the various instabilities in the plasma.

3. LINEAR MODE ANALYSIS

In this section we study the linear evolution of rippling, drift dissipative and radiative condensation instabilities in a plasma, in the presence of a phase sensitive feedback source in the continuity equation and a sheared poloidal flow. We examine analytically the slab eigenmodes of these instabilities in some limiting cases where a linear expansion of the poloidal velocity around the mode rational surface, namely

$$v_0(\xi) = v_0(\xi_s) + \xi v_0'(\xi_s)$$

and $v_0'' = 0$ has been taken. We also investigate in detail the numerical solutions of the rippling and drift dissipative modes, taking a more realistic and general radial profile of the poloidal flow, namely

$$v_0(\xi) = v_0\tanh(\xi/L_u^*) = v_0 f(\xi)$$

where $\xi = 0$ corresponds to the mode rational surface, L_u is the velocity shear scale length and $L_u^* = L_u/a_s$.

3.1. Rippling modes

We start with the simplest derivation of rippling modes driven by impurity gradients alone where $\tilde{t}_e \to 0$ because of large parallel thermal conductivity and $\xi^2/\xi_z^2 \ll 1$ because the impurity parallel diffusion is ignorable. Taking $|\omega| > \omega_*$, so that the pressure gradient effects may be neglected, Eq. (11) leads to the eigenmode equation

$$\left(\frac{d^2}{d\xi^2} + \frac{\tilde{b}}{1-\beta\xi} - \frac{i\tilde{c}\xi^2}{4(1-\beta\xi)} - \frac{\tilde{a}_2\xi}{(1-\beta\xi)^2}\right)\tilde{\phi} = 0 \qquad (14)$$

where we have neglected finite Larmor radius terms,

$$\tilde{b} = -(\omega_*/\bar{\omega})[v_0'(\xi_s)/a_s] - iS_e\omega_*/\tilde{\omega}^2$$

$$\tilde{\omega} = \omega - k_\theta v_0(\xi_s)$$

$$v_0'(\xi) = v_0(\xi_s)/L_u^*$$

$$\beta = k_\theta v_0'(\xi_s)/\tilde{\omega}$$

$$\tilde{c}/4 = \omega_*/\tilde{\omega}\hat{\xi}_R^2$$

$$\hat{\xi}_R^2 = (m_e/m_i)(\nu_{ei}/\omega_*)(L_s^*/L_N^*)^2$$

$$\tilde{a}_2 = \hat{a}_2(\omega_*/\tilde{\omega})^2$$

$$\hat{a}_2 = (U_{\parallel e}/C_s)(L_N^*/L_s^*)(L_N^*/L_z^*)$$

$U_{\parallel e}$ is the directed electron beam velocity and, as before, we have used a linear expansion of the fluid velocity around the mode rational surface: $v_0 = v_0(r_s) + xv_0'(r_s)$. In the absence of velocity shear ($v_0' = 0$) we take $\beta = 0$, and the linear mode width of the rippling instability can be obtained by balancing the $\partial^2/\partial\xi^2$ and ξ^2/ξ_R^2 terms in Eq. (10). This gives

$$\xi_{Rip} \approx (m_e/m_i)(\nu_{ei}/\omega_*)(\omega/\omega_*)(L_s/L_N)^2$$

The eigenmode problem may be exactly solved to give

$$\left(\frac{\gamma_{Rip}}{\gamma}\right)^{5/2} - \left(\frac{\gamma_{Rip}}{\gamma}\right)^{3/2}\left(\frac{\nu_{ei}}{\gamma_{Rip}}\frac{m_e}{m_i}\frac{L_s^2}{L_N^2}\right)^{1/2} \times \frac{|S_e|}{\gamma_{Rip}}\,e^{-i(\pi/2+\phi)} = 1 \qquad (15)$$

where γ_{Rip} denotes the standard rippling mode growth rate [15] in the absence of feedback sources. For $\phi = \pi/2$, the rippling mode growth is reduced, as may be seen by a perturbative calculation of γ as well as a limiting calculation in which $|S_e|$ is so large that the unit magnitude of the RHS may be neglected. When $v_0' \neq 0$, $v_0'' = 0$, we may solve the eigenvalue problem perturbatively to get the following dispersion relation:

$$\left(\frac{\gamma_{Rip}}{\gamma}\right)^{5/2} = 1 - \tilde{b}\theta^{-1/4} - \frac{1}{\beta}\theta^{1/2}[2 + \delta^* + (\delta^* - 1)(\delta^* + 3)Z(\delta^*)] \qquad (16)$$

where $\delta^* = 1 + \theta^{1/4}/\beta$, $\theta = i\tilde{c}/4$ and $Z(\delta^*)$ is the plasma dispersion function with argument δ^*. The weak shear limit corresponds to $\delta^* \to \infty$, and we can use the asymptotic form of the Z function to show that mode stabilization occurs irrespective of the sign of the shear.

In the strong shear limit, we have carried out a detailed numerical analysis of the stability problem. Unfortunately, the simplified analytic approach described above (Eqs (14)–(16)) cannot be extended to the present regime of interest ($\omega \sim \gamma \sim \omega_*$); hence, we have to be satisfied with the numerical results only.

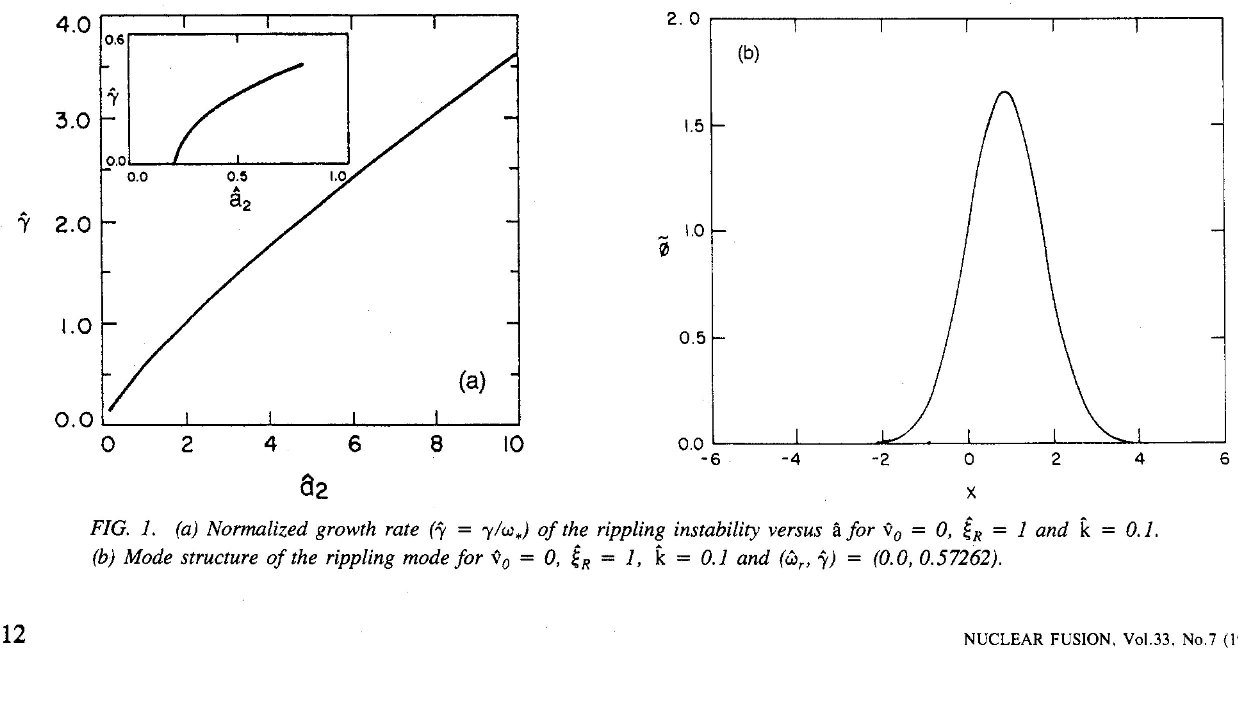

FIG. 1. (a) Normalized growth rate ($\hat{\gamma} = \gamma/\omega_*$) of the rippling instability versus $\hat{a}$ for $\hat{v}_0 = 0$, $\hat{\xi}_R = 1$ and $\hat{k} = 0.1$. (b) Mode structure of the rippling mode for $\hat{v}_0 = 0$, $\hat{\xi}_R = 1$, $\hat{k} = 0.1$ and $(\hat{\omega}_r, \hat{\gamma}) = (0.0, 0.57262)$.

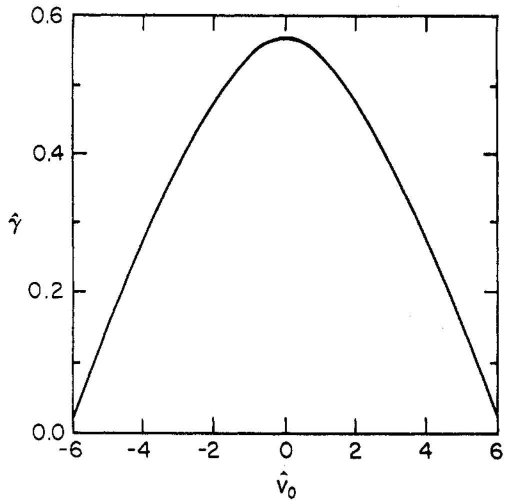

FIG. 2. Growth rate ($\hat{\gamma}$) of the rippling instability versus $\hat{v}_0$ for $\hat{\xi} = 1.0$, $\hat{a} = 1.0$, $\hat{k} = 0.1$ and $L_N^* = 400$.

The eigenvalue equation is recast in a form more convenient for numerical computation:

$$\frac{d^2\tilde{\phi}}{d\xi^2} + Q(\xi)\tilde{\phi} = 0 \tag{17}$$

where

$$Q(\xi) = -\hat{k}^2 - \frac{2\hat{v}_0'(1 - f^2)}{L_u^{*2}(\hat{\omega} - \hat{v}_0 f)}\left(f - \frac{L_u^*}{2L_N^*}\right) - \mathrm{i}\,\frac{\xi^2}{\hat{\xi}_R^2}\,\frac{1}{(\hat{\omega} - \hat{v}_0 f)}\,\frac{\hat{a}_2\xi}{(\hat{\omega} - \hat{v}_0 f)^2}$$

and $\hat{\omega} = \omega/\omega_*$, $\hat{v}_0 = k_\theta v_0/\omega_*$, $L_j^* = a_s/L_j$, $j = u$, s, N and z, $L_u^*/L_N^* > 0$, $\hat{k} = k_\theta a_s$, $S_e = 0$, $v_0'' \neq 0$ and $v_0 = v_0 f(\xi)$. Equation (17) is solved by employing a shooting method with appropriate boundary conditions at large ξ (decaying mode). In Fig. 1(a), we have shown the normalized growth rate $\hat{\gamma}$ as a function of $\hat{a}_2$ for

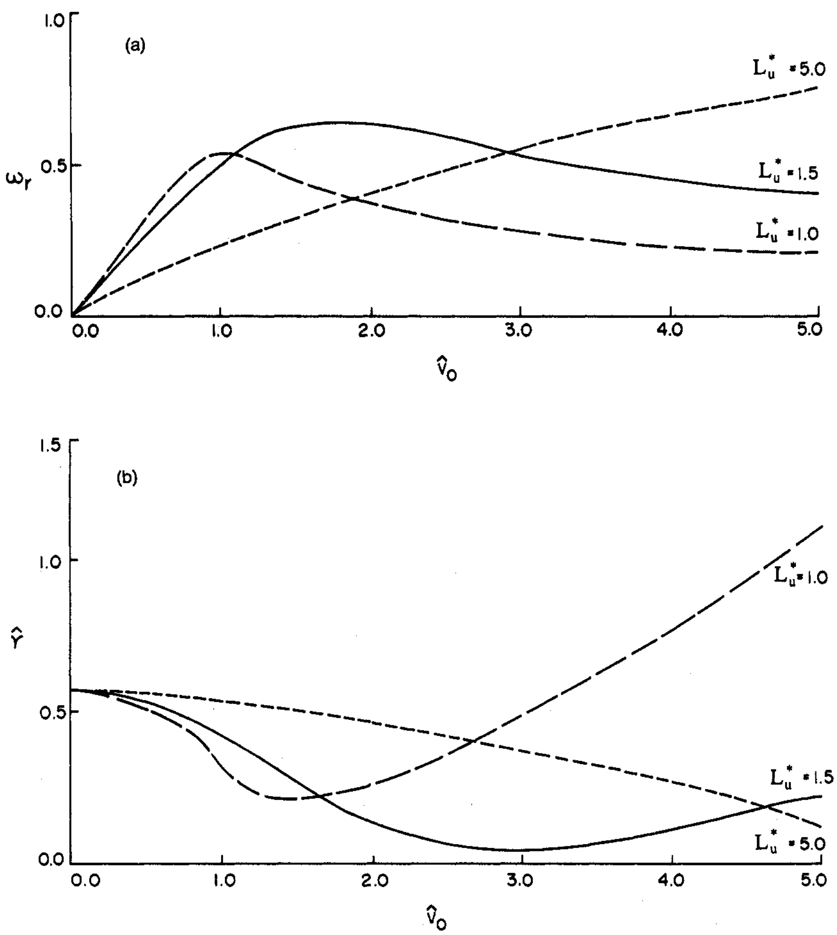

FIG. 3. (a) Real frequency $\hat{\omega}_r$ versus $\hat{v}_0$ and (b) growth rate $\hat{\gamma}$ versus $\hat{v}_0$ of the rippling instability for $\hat{\xi}_R = 1.0$, $\hat{a}_2 = 1.0$, $\hat{k} = 0.1$, $L_N^* = 400$ and $L_u^* = 1.0, 1.5, 5.0$.

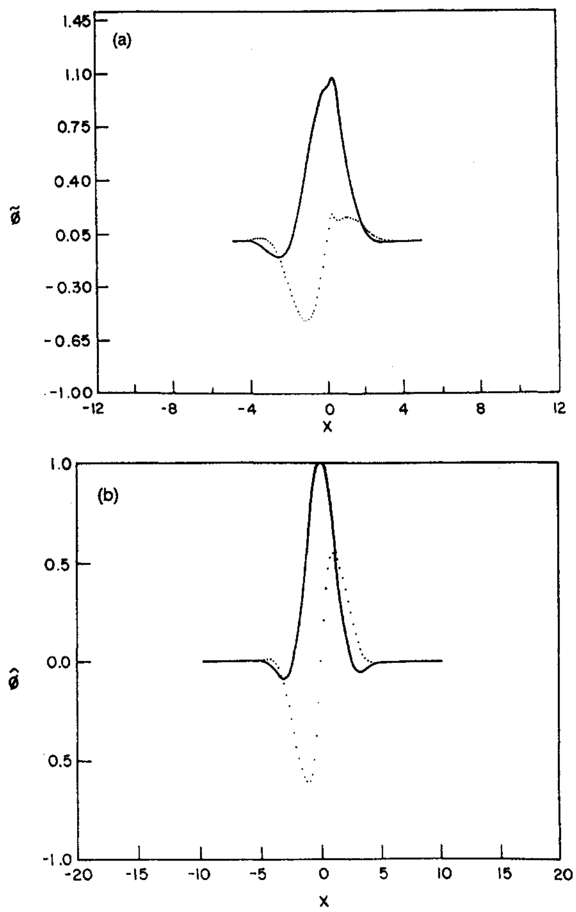

FIG. 4. Mode structure of the rippling mode for (a) $\hat{v}_0 = 1.5$, $(\hat{\omega}_r, \hat{\gamma}) = (0.46028, 0.22498)$, and (b) $\hat{v}_0 = 4.0$, $(\hat{\omega}_r, \hat{\gamma}) = (0.23772, 0.77666)$, with $\hat{\xi}_R = 1$, $\hat{a}_2 = 1.0$, $\hat{k} = 0.1$, $L_N^* = 400$ and $L_u^* = 1.0$.

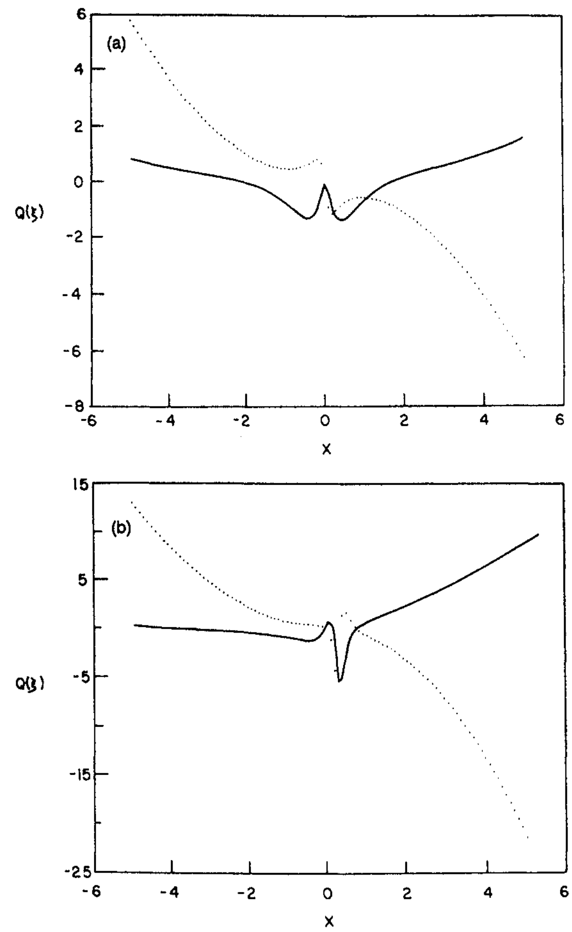

FIG. 5. Schematic plots of the potential function Q of Eq. (17) for $\hat{\xi}_R = 1$, $\hat{a}_2 = 1.0$, $\hat{k} = 0.1$, $L_N^* = 400$ and $L_u^* = 1.0$, with (a) $\hat{v}_0 = 1.5$, $(\hat{\omega}_r, \hat{\gamma}) = (0.46028, 0.22498)$, and (b) $\hat{v}_0 = 4.0$ and $(\hat{\omega}_r, \hat{\gamma}) = (0.23772, 0.77666)$.

$\hat{v}_0 = 0$, $\hat{\xi}_R = 1.0$ and $\hat{k} = 0.1$. The mode structure is displayed in Fig. 1(b). The threshold value for the onset of the rippling instability is found to depend upon the resistive point ($\hat{\xi}_R$) and the normalized parameter ($\hat{a}_2$), which is a function of the scale length of the Z_{eff} gradient. The rippling mode is found to be unstable for $\hat{a}_2/\hat{\xi}_R \geq 0.21$. The introduction of sheared flow is found to have a stabilizing effect on the mode. Our numerical computations show that for parameters typical of tokamak edge plasmas and with the poloidal velocity shear scale length L_u^*, the rippling instability can be suppressed irrespective of whether the flow direction is along the electron diamagnetic drift or opposite to it. This feature is clearly seen in Fig. 2, where the numerical results corresponding to a shear scale length of $L_u^* = 5.0$ are presented. In Figs 3(a) and (b), the real frequency (ω_r) and the growth rate ($\hat{\gamma}$) of the rippling instability are plotted as a function of the normalized flow velocity ($\hat{v}_0$), for three different values of the shear scale length $L_u^* = 1.0$, 1.5 and 5.0. It is seen that sheared poloidal flow has a stabilizing effect over a certain range of flow velocity and that this range varies with the value of the shear scale length. For large values of $\hat{v}_0$, there is a destabilization of the mode. A possible reason for this could be the onset of the Kelvin–Helmholtz instability in this regime [16]. Figure 4(a) shows the mode structure of the unstable rippling mode in the regime where the Kelvin–Helmholtz mode is beginning to emerge ($L_u^* = 1.0$, $\hat{v}_0 = 1.5$). Figure 4(b) shows the mode structure in the regime where the instability is more pronounced (for $\hat{v}_0 = 4.0$). The schematic plots of the potential function Q for these two cases are displayed in Figs 5(a) and (b), respectively.

3.2. Drift dissipative instability

It is well known [17] that in the slab approximation the drift mode is stable in a resistive plasma in a sheared magnetic field. The basic physical reason for this effect is that the magnetic shear gives coupling to parallel sound waves that propagate away from the resonant surface, draining the mode energy resulting in so called shear damping. There are, however, several physical conditions under which the shear damping may be completely suppressed. As examples, we may consider the neutrally stable toroidicity induced eigenmodes discussed by Cheng and Chen [18], or nonlinearly found shear damping suppressed modes [19]. A simple slab eigenmode that also exhibits complete suppression of the shear damping is the one that arises when ω_* has a parabolic profile [17] such that $\omega_*(x) = \omega_*(1 - \xi^2/L_*^2)$ with $L_* \ll \xi_*$, where ξ_* is the ion sound turning point. This simple slab eigenmode can, therefore, reproduce many of the features of the toroidicity induced eigenmodes in a true toroidal plasma. In this section, we consider such a slab eigenmode as a model and investigate the effect of poloidal velocity shear on its stability properties in several limiting cases, namely,

(i) $v_0' = 0$, $S_e \neq 0$,
(ii) $v_0' \neq 0$, $v_0'' = 0$, $S_e = 0$, and
(iii) $S_e = 0$, $v_0'' \neq 0$, $v_0(\xi) = v_0 f(\xi)$.

The appropriate equations may be derived from Eqs (10)–(13), assuming cold ions and $\nabla T_e = 0$. The linear mode width of the drift mode can be approximated by balancing the terms $d^2/d\xi^2$ and ξ^2/ξ_s^2 in Eq. (11). We first write the eigenmode equation for drift waves with feedback terms but $v_0' = 0$:

$$\frac{d^2\tilde{\phi}}{d\xi^2} - \left[1 + \hat{k}^2 - \frac{\omega_*}{\tilde{\omega}}\left(1 - \frac{\xi^2}{L_*^2}\right)\right]\tilde{\phi} - \frac{i\hat{\xi}_R^2}{\xi^2 - i\hat{\xi}_R^2(1 - \hat{S}_\alpha)}\left(1 - \frac{\omega_*}{\tilde{\omega}}\right)\tilde{\phi} = 0 \qquad (18)$$

where $\hat{S}_\alpha = (i|S_e|/\tilde{\omega})\exp(i\phi)$ and we have assumed that $\hat{\xi}_R \ll L_*$. This equation may be solved by the method of matched asymptotic expansions [17] and shows that the growth rate is multiplied by a factor $(1 - \hat{S}_\alpha)^{1/2}$. Thus, for a ϕ such that $\hat{S}_\alpha > 0$ and real, there is a significant reduction of the growth rate using feedback methods. We now consider the case where $\hat{S} = 0$ and $v_0' \neq 0$, so that β dependent terms are important. The new eigenmode equation is

$$\frac{d^2\tilde{\phi}}{d\xi^2} = \left[1 + \hat{k}^2 - \frac{\omega_*}{\tilde{\omega}}\left(1 - \frac{\tilde{\omega}\beta}{k_\theta C_s}\right)\frac{1}{1 - \beta\xi} \times \left(1 - \frac{\xi^2}{L_*^2}\right)\right]\tilde{\phi} + \frac{i\hat{\xi}_R^2(1 - \beta\xi)}{\xi^2 - i\hat{\xi}_R^2(1 - \beta\xi)} \times \left(1 - \frac{\omega_*}{\tilde{\omega}(1 - \beta\xi)}\right)\tilde{\phi} \qquad (19)$$

For $\hat{\xi}_R = 0$, we get the eigenmode equation for the drift wave without resistive effects. If β is small, that is the weak shear case such that $\beta^{-1} > L_*$, the mode is essentially confined by the ω_* variation and the eigenmode has similar properties to the zero shear case. When $0 < \beta^{-1} < L_*$, we get the strong velocity shear case. In this case, we find that the asymptotic behaviour is like $\exp(2i\xi^{3/2}/3\sqrt{\beta L_*^2})$, i.e. like a propagating wave. Again, in this case, we get a shear damped mode.

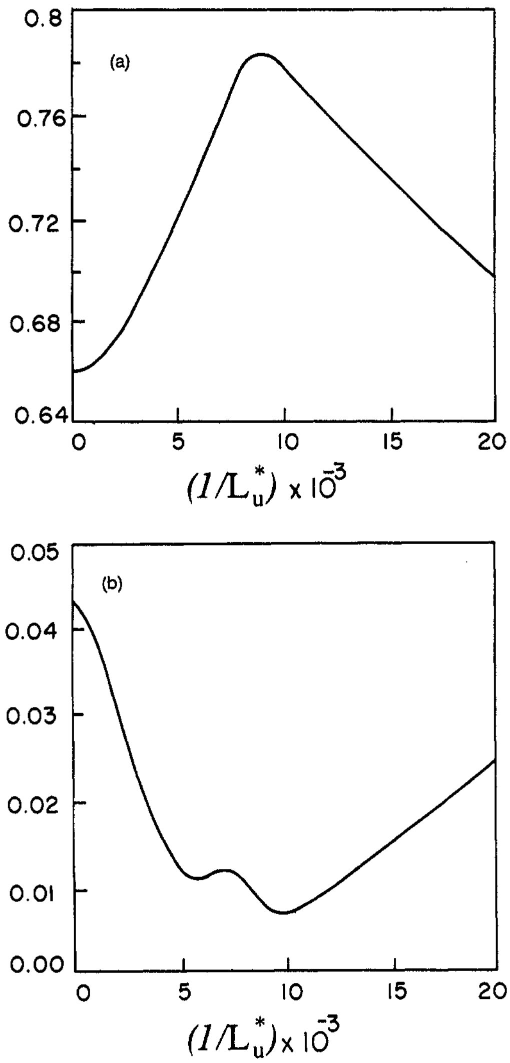

FIG. 6. (a) Real frequency ($\hat{\omega}_r$) and (b) growth rate ($\hat{\gamma}$) for the drift dissipative mode as functions of the shear flow parameter ($1/L_u^*$) with $\hat{v}_0 = 4.0$, $\hat{\xi}_R = 1$, $\hat{k} = 0.1$, $L_N^* = 10$ and $\hat{\xi}_s = 20$.

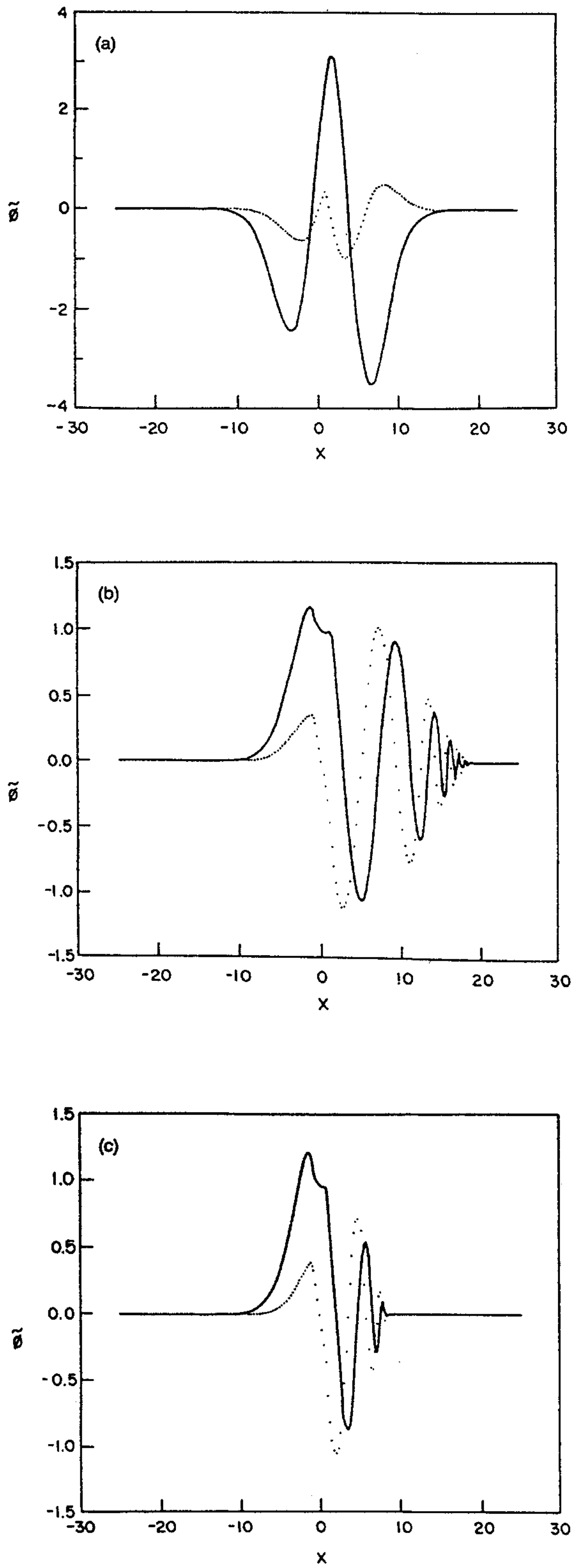

FIG. 7. Mode structure of the drift dissipative mode for $\hat{v}_0 = 4.0$, $\xi_R = 1.0$, $\hat{k} = 0.1$, $L_N^* = 10$ and $\xi_s = 20.0$ for different values of the shear flow parameter: (a) $1/L_u^* = 4.0 \times 10^{-3}$, (b) $1/L_u^* = 1.0 \times 10^{-2}$ and (c) $1/L_u^* = 2.0 \times 10^{-2}$.

For $v_0'' \neq 0$, the eigenvalue equation can again be cast in the form of Eq. (17), where now Q is given by

$$Q(\xi) = -\hat{k}^2 - \frac{2\hat{v}_0'(1 - f^2)}{L_u^{*2}(\hat{\omega} - \hat{v}_0 f)}\left(f - \frac{L_u^*}{2L_N^*}\right) - \frac{\xi^2}{\xi^2 - \mathrm{i}\hat{\xi}_R^2(\hat{\omega} - \hat{v}_0 f)}\left[1 - \frac{1}{(\hat{\omega} - \hat{v}_0 f)} + \frac{\xi^2}{L_u^{*2}(\hat{\omega} - \hat{v}_0 f)} - \frac{\xi^2}{\hat{\xi}_s^2(\hat{\omega} - \hat{v}_0 f)^2}\right]$$

The eigenvalue equation is again solved numerically using a shooting method and the results are displayed in Figs 6 and 7. Figures 6(a) and (b) show plots of the real frequency ($\hat{\omega}_r$) and the growth rate ($\hat{\gamma}$) of the drift dissipative instability as functions of $1/L_u^*$. For typical values of $\hat{v}_0 = 4.0$, $\hat{\xi}_s = 20$, $L_N^* = 10$ and $\hat{\xi}_R = 1.0$, it is seen that shear stabilization is effective in the range of $(L_u^*)^{-1} \leq 0.01$. For larger values, there is further destabilization and the growth rate is found to increase. In Figs 7(a), (b) and (c), we also show the mode structures of the drift dissipative mode for

(i) $(L_u^*)^{-1} = 4.0 \times 10^{-3}$ (stabilized region),
(ii) $(L_u^*)^{-1} = 1.0 \times 10^{-2}$ (region of minimal growth) and
(iii) $(L_u^*)^{-1} = 2.0 \times 10^{-2}$ (region of shear destabilization).

3.3. Radiative condensation instability

In this section, we investigate the radiative condensation instability [20, 21] which is an important candidate for short scale length fluctuations (poloidal mode number $m \gg 1$) in tokamak edge plasmas. Physically, this instability is caused by $\partial L/\partial T_e < 0$ and $L \propto N^2$ and leads to the development of cold spots of high density. The mode that is dominantly driven by radiative condensation effects is typically important when the edge plasma has a high electron density and is formed away from the mode rational surface where $k_\| C_s \gg \omega$ (this is to be distinguished from other small $k_\|$ modes such as rippling modes, whose growth rate could be influenced by radiative effects). We shall concentrate our attention on this mode. The radial extent of the mode can be estimated by balancing the parallel and perpendicular thermal conductivities and gives $\xi_{rad} \approx (\chi_{\perp e} L_s^2/k_y^2 \chi_{\| i})^{1/4}$. We now study the effect of sheared poloidal flow and an active feedback source term. For $\nabla N = \nabla T = 0$, $k_\|^2 C_s^2/\bar{\omega}^2 > 1$, $m_e \nu_{ei}/m_i \bar{\omega} > 1$, we find, by adding the electron and ion energy equations (because the electrons and ions are strongly coupled) and using the condition that $\tilde{p} = \tilde{p}_e + \tilde{p}_i \cong 0$, the eigenmode equation

$$\left[\frac{\partial^2}{\partial \xi^2} - k_\theta^2 a_s^2 + \xi_{k\perp i}^2 \left(\hat{\gamma}_n + \hat{\gamma}_T - 1.14\mathrm{i}S_e - \frac{\xi^2}{\xi_{k\parallel e}^2}\right) + 2\mathrm{i}(1 - \hat{\beta}\xi)\xi_{k\perp i}^2\right]\tilde{t}_e = 0 \qquad (20)$$

This is a standard Hermitian equation, which yields the eigenvalue condition

$$\omega_r = k_\theta v_0(r_s) \qquad (21)$$

$$\gamma = \frac{1}{3}\left(\frac{2L}{NT} - \frac{1}{N}\frac{\partial L}{\partial T}\right) - \frac{1}{3}\left(\frac{k_\theta^2}{L_s^2}\chi_{\perp i}\chi_{\parallel e}\right)^{1/2} - \frac{1}{3}k_\theta^2\chi_{\perp i} - \frac{3}{4}\left(\frac{v_0'^2 L_s^2}{\chi_{\parallel e}}\right) - 0.57|S_e|\exp[\mathrm{i}(\pi + \phi)] \qquad (22)$$

It may be noted that the velocity shear produces a stabilizing effect on the growth irrespective of the sign. The feedback term is found to be stabilizing for $\phi = -\pi$.

Finally, a brief discussion is in order on the manner in which a density feedback source/sink could be conveniently introduced into the plasma edge region. A particularly simple way is to use poloidally asymmetric biasing of electrically isolated individual limiter tiles. Alternatively, one could use several biased probes at appropriately chosen locations in r and θ. The (r, θ) variation of the density sink/source will then depend on how well the biasing potential at its oscillating frequency is shielded/propagated by the plasma. The method should be quite effective for the scrape-off layer as well as the outer part of the plasma inside the last closed magnetic surface. It should be emphasized that the linear analysis of feedback discussed in our paper simply Fourier analyses the source/sink term and converts it into an $S(k, \omega)$. This means that modifications of the (r, θ) structure of the true density source/sink can only be utilized to improve the efficient coupling to the desired (k, ω) values.

4. CONCLUSIONS

We have investigated the linear stability of the rippling modes, the radiative condensation instabilities, and the drift dissipative mode in the presence of a sheared poloidal flow and of a phase sensitive feedback source. The latter is introduced in the electron continuity equation, and the conditions for the stabilization of the modes are obtained by a combination of analytic and numerical analysis of the relevant eigenmode equations. For a simple linear velocity profile, namely $v_0 = v_0(r_s) + xv_0'(r_s)$, analytic methods show that for weak shear, the stabilization is independent of the sign of v_0'. A more general poloidal flow profile, namely $v_0(\xi) = v_0 \tanh(\xi/L_u^*)$, is employed to study the strong shear limit, and the eigenmode equations are solved numerically in this case. It is found that both the rippling and the drift dissipative modes can be suppressed with sheared poloidal flow irrespective of the flow direction. The stabilization occurs over a range of flow velocities that depends on the value of the scale length. The unstable regime beyond a certain flow velocity value is possibly due to the onset of the Kelvin–Helmholtz instability [16]. We find the onset of this regime for typical values of $\hat{v}_0 \approx 1.5$, $L_u^* \leq 5$ for the rippling mode and of $\hat{v}_0 \approx 4.0$, $L_u^* \leq 50$ for the drift dissipative mode. We also find that a poloidal sheared flow, with a simple linear velocity profile, stabilizes the radiative condensation mode irrespective of the sign of the shear. The feedback source in the electron continuity equation can bring about stabilization for a phase of $-\pi$.

REFERENCES

[1] STANGEBY, P.C., McCRACKEN, G.M., Nucl. Fusion **30** (1990) 1225.
[2] RITZ, C.P., et al., Nucl. Fusion **27** (1987) 1125.
[3] SAMM, U., et al., Plasma Phys. Control. Fusion **29** (1987) 1321.
[4] TAYLOR, R.J., et al., Phys. Rev. Lett. **63** (1989) 2365.
[5] GROEBNER, R.J., et al., Phys. Rev. Lett. **64** (1990) 3015.
[6] RITZ, C.P., et al., Phys. Rev. Lett. **65** (1990) 2443.
[7] SHAING, K.C., et al., Plasma Physics and Controlled Nuclear Fusion Research 1988 (Proc. 12th Int. Conf. Nice, 1988), Vol. 2, IAEA, Vienna (1989) 13;
KIM, Y.B., et al., Phys. Fluids B **2** (1990) 2143.
[8] CHU, T.K., HENDEL, H.W. (Eds), Feedback and Dynamic Control of Plasmas, AIP Conference Proceedings, No. 1, American Institute of Physics, New York (1970).
[9] OTT, E., et al., Phys. Rev. Lett. **64** (1990) 1196;
DITTO, W.L., et al., Phys. Rev. Lett. **65** (1990) 3211.
[10] JHA, R., et al., Phys. Rev. Lett. **69** (1992) 1375.
[11] SINGH, R., et al., in Research Using Small Tokamaks, IAEA-TECDOC-604, IAEA, Vienna (1991) 97.
[12] SUGAMA, H., WAKATANI, M., Phys. Fluids B **3** (1991) 1110.
[13] BRAGINSKII, S.I., in Reviews of Plasma Physics, Vol. 1 (LEONTOVICH, M.A., Ed.), Consultants Bureau, New York (1965) 205.
[14] RUTHERFORD, P.H., in Physics of Plasma close to Thermonuclear Conditions (Proc. Course Varenna, 1979), CEC, Brussels (1980) 143.
[15] ROGISTER, A., Plasma Phys. Control. Fusion **26** (1984) 1063.

[16] WEYNANTS, R.R., et al., Nucl. Fusion **32** (1992) 837 (and references therein).
[17] CHEN, L., et al., Nucl. Fusion **19** (1979) 373.
[18] CHENG, C.Z., CHEN, L., Phys. Fluids **23** (1980) 1770.
[19] BISKAMP, D., WALTER, M., Phys. Lett. A **109** (1985) 34.
[20] SINGH, R., et al., Nucl. Fusion **32** (1992) 379 (and references therein).
[21] DRAKE, J.F., et al., Phys. Fluids **31** (1988) 813.

(Manuscript received 28 September 1992
Final manuscript received 17 May 1993)